Progress in Organic Coatings 204 (2025) 109186

Contents lists available at ScienceDirect

Progress in Organic Coatings

journal homepage: www.elsevier.com/locate/porgcoat

A hierarchically amphiphobic structure enables coating an extraordinary anti-corrosion performance

Zhaowen Tian [a,1], Ruiyu Ma [a,d,1], Yiqing Chen [b,*], Suning Li [a,c], Hongwei Zhao [a], Yanqiu Zhang [a], Qingdong Li [d], Xueyuan Zhang [d], Baigang An [a,*]

[a] Key Laboratory of Energy Materials and Electrochemistry Liaoning Province, School of Chemical Engineering, University of Science and Technology Liaoning, Anshan 114051, China
[b] State Key Laboratory of Metal Material for Marine Equipment and Application, Anshan 114009, China
[c] School of Chemical Engineering, Nanjing University of Science and Technology, Nanjing, Jiangsu 210094, PR China
[d] Institute of Corrosion Science and Technology, Guangzhou 510530, China

ARTICLE INFO

Keywords:
Amphiphobic coatings
Underwater oleophobicity
Anti-corrosion
Polydopamine/polyethylenimine
Carboxylated carbon nanotubes

ABSTRACT

Amphiphobic coatings have great potential in anti-corrosion coatings, oil-water separation, and so on. These are usually achieved by building multistage micron/nanometer roughness or re-entrant curvature surface through low surface energy materials. However, the complexity and mechanical brittleness of amphiphobic coatings derived from surface micro/nano structures have long posed challenges to their practical application. Here, we constructed a hierarchical structure coating with amphiphobic properties using polydopamine/polyethylenimine (PDE) as a connecting layer between the 1H,1H,2H,2H-perfluorodecyltriethoxysilane (PFDTES)-modified epoxy coating (POS-EP) and the carboxylated carbon nanotube (CNTs-COOH) modified epoxy coating (CNTs-EP) via dip-coating technology. CNTs-COOH addition reduces the porosity defects in the epoxy resin and impart hydrophilicity to the coating, demonstrating excellent underwater oleophobicity (OCA = 134.6°), thereby preventing the POS-EP coating from being eroded by oily organic substances in aqueous environments. PFDTES is employed to enhance the hydrophobicity of the epoxy resin, improving the coating's impermeability and corrosion resistance, with a water contact angle of 127.2° on its smooth surface. Surface morphology and elemental analysis confirm the seamless connection of the hydrophobic and hydrophilic layers facilitated by the PDE transition layer. Consequently, the amphiphobic coating with the hierarchical structure exhibits outstanding anti-corrosion performance. Compared to the epoxy resin coatings, the amphiphobic coating's resistance (R_c) and low-frequency modulus ($|Z|_{0.01Hz}$) are improved by 2 to 4 orders of magnitude after 60 days of immersion testing in 3.5 wt% NaCl and 18 days of neutral salt spray tests. Even the coating suffered the local damages, the synergistic effects between the amphiphobic interface can still hinder the attacks of corrosion media, and thus continues to supply good anti-corrosion properties. Given its low cost, scalability, and durability, this novel coating is expected to pave new avenues for the construction of various amphiphobic coatings.

1. Introduction

Amphiphobicity is a natural phenomenon in that one substance owns both hydrophobicity and oleophobicity. For example, springtail skin owns the repellency for both water and oil [1]. Lotus leaf whose upside is superhydrophobicity but the down side is superoleophobicity [2] The amphiphobicity of materials comes from their low surface energy and special surface micro/nanostructures [3–6]. In past decades, the amphiphobic materials have been extensively developed in some fields of self-cleaning, anti-fingerprinting, anti-fouling, anti-corrosion, and anti-icing applications [7–12]. Particularly, the amphiphobic coatings can effectively inhibit the penetration of both oleiferous and aqueous corrosion media [13,14] to well protect the metal matrix from corrosion. Therefore, it is highly expected to design anticorrosion materials with the amphiphobicity.

Solid materials with low surface tension generally own hydrophobicity in essence, but they are generally oleophilic and thus are susceptive to suffer from the attack of organic pollutants and

* Corresponding authors.
E-mail addresses: chenyiqing@ansteel.com.cn (Y. Chen), bgan@ustl.edu.cn (B. An).
[1] The two authors contribute equally to this work.

https://doi.org/10.1016/j.porgcoat.2025.109186
Received 20 January 2025; Received in revised form 23 February 2025; Accepted 28 February 2025
Available online 9 March 2025

microorganisms [8,15], such as crude oil contaminations and industrial oily wastewater. For example, Zhao et al. synthesized a branched epoxy resin through a Michael addition reaction and successfully fabricated a superhydrophobic coating on cotton fabric by curing it epoxy with hydrophobic SiO_2 nanoparticles, triethylenetetramine, and (3-aminopropyl) triethoxysilane. However, the coating exhibited strong oleophilicity [16]. Wei et al. sprayed a homogeneous suspension containing the cetyl polysiloxane-modified silica nanoparticles onto the cured epoxy resin surface to form a superhydrophobic coating [17], but oily pollutants easily eroded the coating. The main reason for these cases is that most organic materials have ultra-low surface tension, making fabricating an oleophobic surface difficult.

As being inspired by natural biology like springtail, special surface roughness constructed by a variety of nano-micro structures can endow materials an oleophobicity [2,15,18]. Zhao et al. firstly constructed a micro-column array structure on a silicon substrate by an etching process, which was then coated with the fluorosilane layer, the material as prepared showed strong amphiphobicity [19]. Maesoon et al. fabricated an inverted trapezoidal microstructure array on the surface of a transparent polydimethylsiloxane (PDMS) elastomer using backside three-dimensional (3D) diffractive lithography and template replication technology, after being coated with Teflon, the surface becomes both oil and water-repellent [20]. Kim et al. devised a superamphiphobic structure by intertwining TiO_2 nanotubes with a diameter of 8 nm on the microtextured Ti surface through a straightforward electrochemical etching and the subsequent hydrothermal treatment process [21]. Although combining the micro-nanostructure with the low surface energy material can bring an amphiphobic coating, a critical drawback is that the micro/nanoscale porous structure causes the coatings to have weak mechanical strength and brittleness [22]. Once the microstructure was destroyed, the coatings would loss amphiphobicity to degrade the anticorrosion performance. Therefore, the coatings constructed by low surface energy materials and nano-micro structures are inefficient in anticorrosion properties and complicated in the preparation process. An innovative amphiphobicity structure is highly expected for anticorrosion coatings.

Generally, materials suffer from aqueous corrosion environments, the compactness and mechanical strength of coatings are especially important to obstruct the hydrated corrosive ions and the erosive particles, but such materials are generally hydrophilic. However, conventional coatings are typically subject to contamination by some oily organics in aqueous environments. Consequently, the coatings are also needed to possess underwater oleophobicity. Du et al. engineered a durable underwater superoleophobic coating through the deposition of a composite of polyethyleneimine and titanium dioxide upon the epoxy resin substrate. The coating exhibits favourable antifouling and anticorrosion properties [23]. Furthermore, once the coating was locally broken, in which the hydrated ions could penetrate through the coatings to attack the protected metals, if a hydrophobicity can be provided at this period by coating, the aqueous matters would be blocked by the hydrophobic layer of coating and thus the matrixes were well protected. How to give coating this physical properties and functions requires an innovative design.

In this study, a hierarchically amphiphobic coating has been designed and prepared on the surface of Q235 carbon steel. The coating is composed of a hydrophobic layer of PFDTES modified epoxy resin and an underwater oleophobic layer of CNTs-COOH modified epoxy resin, they seamlessly connected through a highly adhesive transition layer of PDE to construct the hierarchical amphiphobic coating of POS-EP/PDE/CNTs-EP. The underwater oleophobic CNTs-EP layer effectively resists the corrosion of Q235 carbon steel caused by organic pollutants in water, while its low porosity defects can physically block the penetration of water and ions. Furthermore, even if small amounts of water-soluble substances penetrate the coating, the hydrophobic POS-EP layer can repel water molecules, thereby providing further protection to the metal substrate against corrosion. In the event of local damage to both the hydrophobic and hydrophilic phases, the additional pressure generated at the interface between these two phases can effectively suppresses further corrosion of the Q235 carbon steel substrate. Consequently, the amphiphobic POS-EP/PDE/CNTs-EP coating exhibits excellent underwater oleophobicity and extraordinary corrosion resistance.

2. Experimental

2.1. Reagents

Ethanol and hydrochloric acid were purchased from Sinopharm Chemical Reagent Co., Ltd. Dimethyl sulfoxide was purchased from Liaoning Quanrui Reagent Co., Ltd. Tris(hydroxymethyl)aminomethane was purchased from Shanghai Aladdin Reagent Co., Ltd. Epoxy resin (E44), curing agent (704), polyethyleneimine (PEI) and PFDTES were provided by Shanghai Macklin Biochemical Co., Ltd. Dopamine Hydrochloride were provided by Shanghai Titan Technology Co., Ltd. Graphitized Carboxyl Multi-walled carbon nanotubes (MWCNTs, diameter 10–20 nm, length 5–30 μm) are provided by Xianfeng Nanomaterials Technology Co., Ltd.

2.2. Preparation of coatings

2.2.1. Hydrophobic POS-EP coating

The epoxy resin (2.0 g) and ethanol (5.0 g) were mixed with stirring at room temperature for 2 h, then an ethanol solution (60 μL/g) containing PFDTES was added with continuous stirring for 2 h. Subsequently, polyamide hardener (2.0 g) was mixed with ethanol (5.0 g), and then which was added into the above-mentioned mixture with stirring for 2 h to form a homogeneously hydrophobic epoxy solution. The hydrophobic coating was prepared on the surface of Q235 carbon steel using a dipping machine at a speed of 1 mm/min. The process involved two dipping cycles, followed by pre-curing at room temperature for 12 h. Subsequently, the coating was subjected to further heating in air at 80 °C for 2 h to get the POS-EP coating.

2.2.2. CNTs-EP coating

2.0 g of epoxy resin were added into 5.0 g of ethanol accompanying with stirring for 2 h. Then, 150 mg of CNTs were ultrasonically dispersed in 2.50 g of ethanol for 20 min before being added into the previously prepared solution. This mixture was stirred for another 2 h, followed by the addition of a 5.0 g ethanol solution containing 2.0 g of polyamide curing agent, which was stirred for 1 h to form a uniform CNTs-modified epoxy resin solution. The underwater oleophobicity coating was prepared on the surface of Q235 carbon steel using a dipping machine at a speed of 1 mm/min. The process involved two dipping cycles, followed by pre-curing at room temperature for 12 h. Subsequently, the coating was subjected to further heating in air at 80 °C for 2 h, resulting in a CNTs-EP coating.

2.2.3. POS-EP/PDE coating

Dopamine hydrochloride (100 mg) and polyethyleneimine (100 mg) were added to 50 mL tris(hydroxymethyl) aminomethane buffer solution at pH of 8.5. The POS-EP coating was immersed in the solution and oscillated for 2 h. Thereafter, the coating was subjected to a thorough rinsing with deionized water and subsequently dried at 80 °C for 2 h resulting in the formation of a PDE functionalized POS-EP coating (POS-EP/PDE).

2.2.4. POS-EP/PDE/CNTs-EP coating

According to the above process, POS-EP, PDE transition layer and CNTs-EP coating were sequentially coated on the surface of Q235 carbon steel to obtain POS-EP/PDE/CNTs-EP coating. In order to ensure that the thickness of all tested coatings is consistent, a coating thickness gauge (MC-3000S) with a resolution of 0.1 μm is used. The thickness of all coatings is kept at 60 ± 5 μm.

2.3. Materials characterization

The surface morphologies of samples were observed by field emission scanning electron microscope (SEM, Apreos, USA) under the condition of accelerating voltage 10 kV and accelerating current 13 PA. The surface chemical composition of samples was analyzed by X-ray photoelectron spectroscopy (XPS, AXIS-SUPRA) and Fourier transform infrared spectroscopy (Alpha II, BRUKER). The XPS spectra were recorded in the constant energy mode of 20.0 eV, and all the binding energies were calibrated with the C1s peak of 284.5 eV as the reference. The water contact angle (4 mL droplet volume) on the coating surface was measured using a contact angle meter (SCD-200S) to analyze the wettability of the coating surface. At least 3 positions were tested for each coating.

2.4. Anticorrosion performance tests

In order to evaluate the anti-corrosion performance of the coatings, the electrochemical tests were carried out in 3.5 wt% sodium chloride simulated seawater. All electrochemical tests were carried out on the electrochemical test system (Gamry Interface 1010E). The testing system is a typical three-electrode configuration, comprising a reference electrode (Ag/AgCl), a counter electrode (platinum sheet), and a working electrode (Q235 carbon steel), with a frequency range spanning from 10^4 Hz to 10^{-2} Hz. The tests were carried out in self-made Faraday cages to avoid the external interference. The frequency range of the electrochemical impedance (EIS) test is from 10 kHz to 0.01 Hz, and the interference voltage is 20 mV. The scanning speed of the potential polarization curve is 1.0 m V/s. The corrosion current density of I_{corr} and corrosion potential of E_{corr} were obtained by linear extrapolation fitting of polarization curves. The accelerated corrosion tests of the coatings were carried out in the salt spray test chamber (T-YW-60, Dongguan Tianyi Environmental Testing Instrument Co., Ltd.), EIS measurements and photographic documentation of the samples were conducted at predetermined time intervals.

3. Results and discussion

3.1. Functional modification and surface wettability of coatings

The preparation of POS-EP/PDE/CNTs-EP coatings is schematically shown in Fig. 1. Firstly, a POS-EP coating was prepared by incorporating PFDTES into a mixture of epoxy resin and polyamide curing agent. To achieve a seamless connection of the POS-EP layer with the CNTs-EP layer, the prepared POS-EP coating was immersed in an aqueous solution of polydopamine and polyethyleneimine to get a bioinspired transition layer of PDE with abundant hydroxyl groups on the surface. Finally, a CNTs-EP coating was prepared on the surface of the PDE transition layer to construct a hierarchically amphiphobic POS-EP/PDE/CNTs-EP coating on the Q235 steel.

As shown in Fig. 2a–c, compared to with the brittle fracture and porous defects surface of epoxy coating, both the POS-EP coating and CNTs-EP coating show more compactness and the fewer defects. The uniformly dispersed CNTs in the epoxy resin can be observed. The chemical surface state of coatings was analyzed by XPS, and the results are shown in Fig. 2d. Compared with EP or CNT/EP coating, POS-EP coating shows an additional F1s peak (689.3 eV) with an atomic content of 60.57 % (Table S1). The C1s spectrum (Fig. S1) shows that the signal at 289.9 and 291.9 eV corresponds to the C-F_2 and C-F_3 peaks of POS-EP coating [24], which results in the hydrophobic surface POS-EP coating (Fig. 2e) with low surface energy. The atomic force microscopy (AFM) images (Fig. S2) observed that the coating has a “smooth” surface, further confirming that the hydrophobicity of the POS-EP coating is primarily attributed to the successful modification with fluorine-functional groups.

However, the coatings with low surface energy generally have weak surface adhesion properties [7,17,25]. The high adhesion PDE transition layer was used to modify the surface of the POS-EP coating to make a seamless connection between CNT/EP and POS-EP. Fig. 2d shows the XPS survey spectra of samples. Compared with POS-EP, the atomic F1s content in POS-EP/PDE decreases from 60.57 % to 28.84 %, an additional N 1s peak appears at 399.2 eV, which can be deconvoluted into C—N (398.1 eV) and N—H (399.9 eV) (Fig. S3), attributed to the amino groups in the PDE transition layer [26,27]. Furthermore, the contact angles (CAs) decreases to 87.8° (Fig. 2e), suggesting that a large amount of hydroxyl and amino groups introduced by the PDE transition layer has resulted the change from hydrophobic to hydrophilic surface on the coating. It can be confirmed by the Fourier-transform infrared spectroscopy (FTIR) of Fig. S4. Two absorption peaks at 3287 and 3346 cm^{-1} are attributed to the stretching vibrations of the —N—H bonds. The absorption peak observed at 3325 cm^{-1} corresponds to the stretching vibration of hydroxyl (-OH) groups within the PDE transition layer [28,29]. In Fig. S5, the C 1s peak of CNTs-EP can be deconvoluted into C—C (284.6 eV), C═O (286.1 eV), and O—C═O (287.7 eV) bonds [30]. Compared to the EP coating, the modification of the epoxy resin with CNTs-COOH increases the atomic concentration of O 1s from 11.88 % to 13.21 % (Table S1), resulting in the higher surface energy for the CNTs-EP coating. Consequently, a reduction in the contact angle (CA) from

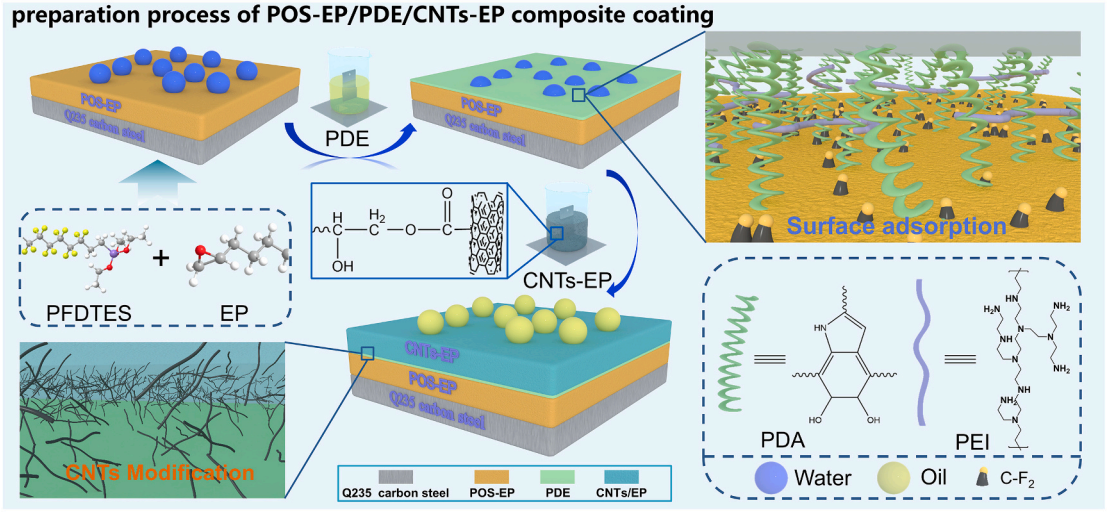

Fig. 1. Schematic preparation of amphiphobic coating with a hierarchical structure of POS-EP/PDE/CNTs-EP.

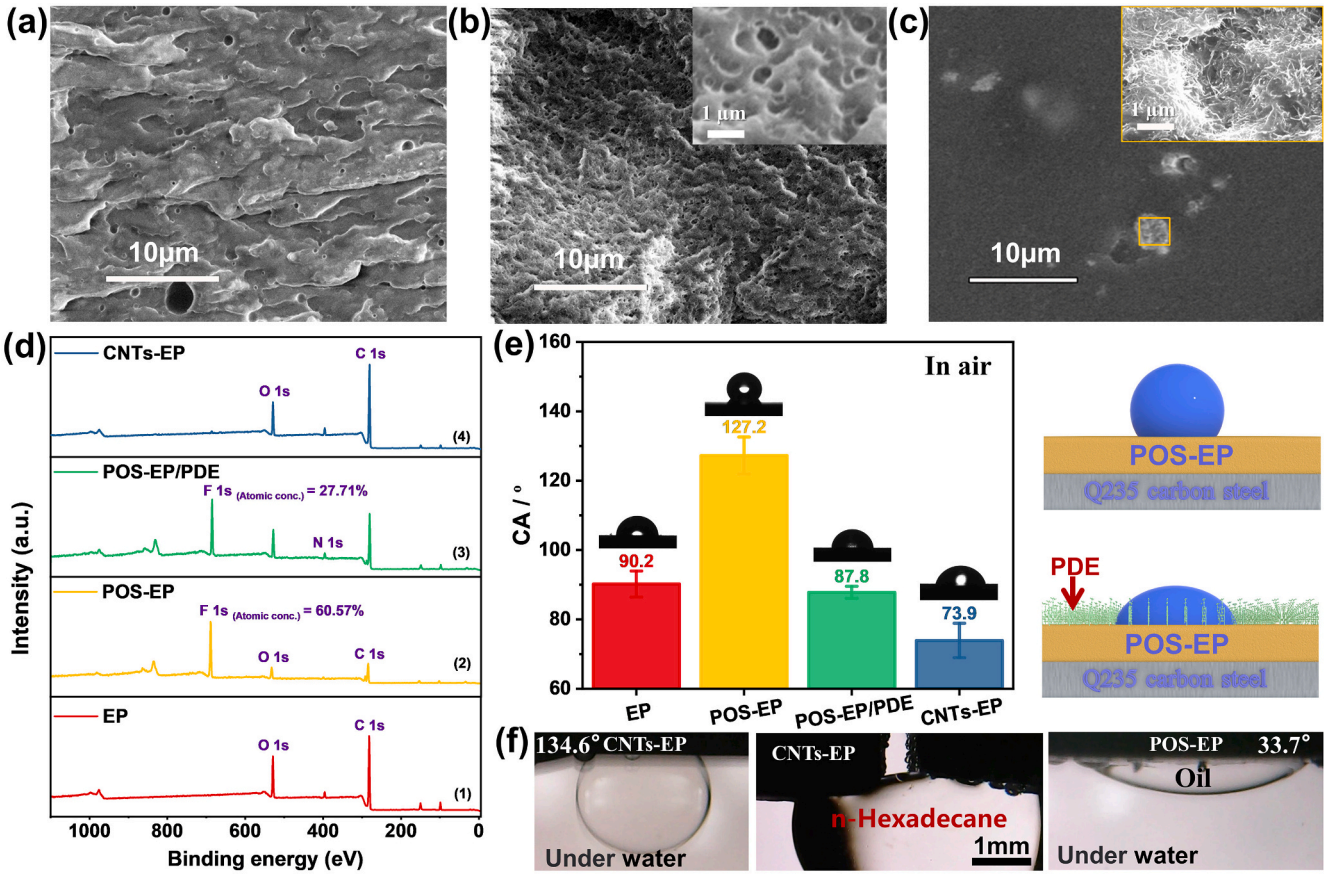

Fig. 2. SEM images of (a) EP coating, (b) POS-EP coating and (c) CNTs-EP coating, (d) Full X-ray photoelectron spectrum of EP coating, POS-EP coating, POS-EP-DE coating and CNTs-EP coating, (e) static contact angles of water droplets on the surfaces of EP, POS-EP, POS-EP/PDE and CNTs-EP coatings (4 μL), (f) Static contact angle of CNTs-EP coating and POS-EP coating with n-hexadecane under water.

90.2° to 73.9° (Fig. 2e) makes the coatings easier to be wetted by water.

CNTs-EP coatings was assessed by using contact angle goniometry. In Fig. 2f, it can be observed that the CNT/EP coating has a high static CA of 134° with the n-Hexadecane ($\gamma = 27.2$ mN/m) distributed in water. Surprisingly, even when the coating has millimetre-scale defects, the penetration of low surface tension liquids can still be inhibited. However, the static contact angle POS-EP coating with n-hexadecane in water is only 33.7° (Fig. 2f), making it more susceptible to erosion by low surface tension liquids.

3.2. *Interface stability of hierarchically amphiphobic coatings*

Since there are big differences between the POS-EP layer and CNTs-EP layer, how to get an effective connection and good interface stability of the layers is critical for the preparation of the amphiphobic coating with good anti-corrosion performance. As confirmed by XPS (Fig. 2d), a transition layer of PDE endowed the POS-EP coating with a large number of hydroxyl and amino groups, which can result in a strong interaction with the CNTs-EP coating containing oxygen functional groups. The cross-sectional area of coatings with and without using PDE as the transition layer were observed and analyzed, the results are shown in Fig. 3. From an optical microscopy, it is difficult to distinguish the area connecting POS-EP with CNTs-EP (Fig. 3a, c). However, the gap with a width of about 6.0 μm between POS-EP and CNTs-EP can be clearly found by SEM (Fig. 3b) when there is no PDE transition layer. In contrast, when a PDE transition layer was used, a seamless connection between CNTs-EP and POS-EP can be achieved, there is no any gaps to be observed (Fig. 3d). As illustrated by Fig. 3e and f, PDE can provide numerous hydrogen bonds between the two coatings to produce a strong interfacial adhesion. But only a weak intermolecular force can be formed when there is no PDE layer. Moreover, Energy dispersive spectrometer (EDS) also demonstrate a smooth distribution of elemental O and C comparing to the coating without using the PDE modification. The results confirm that the PDE transition layer effectively facilitates a seamless connection between the oleophobic CNTs-EP and the hydrophobic POS-EP to construct a hierarchically amphiphobic POS-EP/PDE/CNTs-EP coating, which is expected to provide satisfactory anticorrosion performance.

3.3. *Anticorrosive behavior of coatings*

The anticorrosion behavior of coatings was evaluated by electrochemical impedance spectroscopy (EIS). The impedance modulus of coating at low frequency ($|Z|_{0.01Hz}$) is an important parameter to evaluate the anti-corrosion performance of materials. The higher the value of $|Z|_{0.01Hz}$ generally represents the better the anticorrosive effect of the coating [31]. In Fig. 4a1, $|Z|_{0.01Hz}$ value of EP coating gradually decreases with immersion time, which is 1.02×10^{10} Ω cm^2 after 5 days of immersion and then sharply drops to 5.76×10^{7} Ω cm^2 after 60 days, indicating that the protective performance of EP coating degraded. Additionally, the phase angle plots displayed two-time constants (Fig. 4a2), suggesting a significant diffusion phenomenon appeared at low frequency (Fig. S6a), due to the corrosive substances diffused along the coating defects [32]. In Fig. 4b1, the $|Z|_{0.01Hz}$ value of POS-EP coating is 4.52×10^{8} Ω cm^2 after 60 days of immersion, which is about one order of magnitude higher than EP coating. The phase angle plot showed a one-time constant (Fig. 4b2), indicating that no diffusion phenomena occurred (Fig. S6b). The results confirm that the

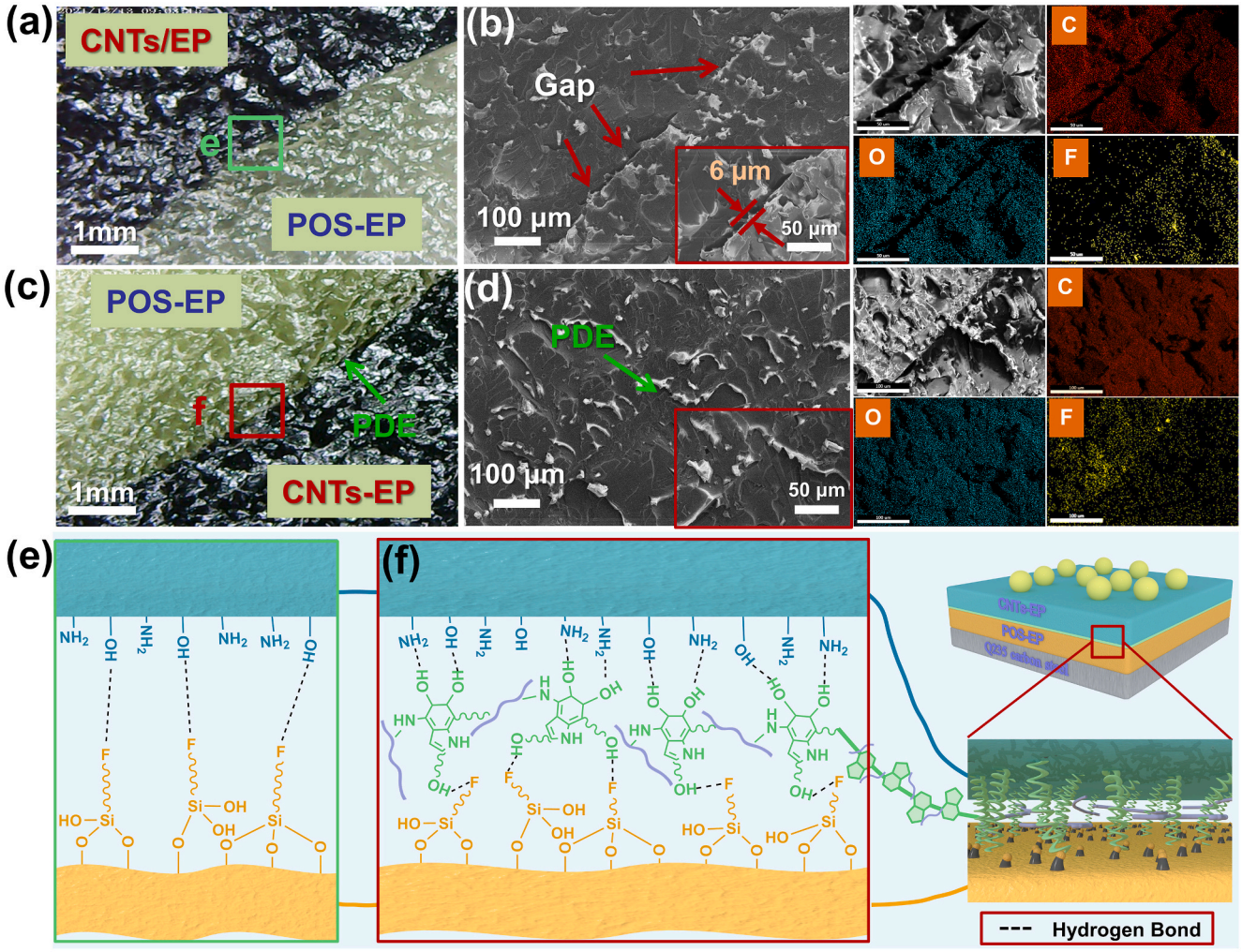

Fig. 3. Optical photos of macroscopic state hierarchically structured POS-EP/CNTs-EP coating (a) and POS-EP/PDE/CNTs-EP coating (c), SEM images and EDS elemental maps POS-EP/CNTs-EP coating (b) and POS-EP/PDE/CNTs-EP coating (d), Interaction principle of amphoteric coating interface without PDE transition layer (e) and with PDE transition layer (f).

hydrophobic modification on EP by PFDTES improves the protective properties of the coating.

$|Z|_{0.01Hz}$ value of CNTs-EP coating is 8.77×10^9 Ω cm^2 after 5 days (Fig. 4c1), and then slightly decrease to 2.75×10^8 Ω cm^2 after 60 days. The phase angle plot still showed one time constant with no diffusion phenomena (Figs. 4c2, S6c), indicating that the introduction of CNTs significantly improved the corrosion resistance of the coating by reducing the porosity defects. The amphiphobic coating of POS-EP/PDE/CNTs-EP exhibited much better anticorrosion property than the POS/EP coating ($|Z|_{0.01Hz} = 4.52 \times 10^8$ Ω cm^2) and CNTs-EP coating ($|Z|_{0.01Hz} = 2.75 \times 10^8$ Ω cm^2), whose $|Z|_{0.01Hz}$ value slightly decreased from 3.81×10^{10} Ω cm^2 to 5.63×10^9 Ω cm^2 after 60 days immersion (Fig. 4d1) and the phase angle plots maintained one time-constants (Fig. 4d2). The significant improvement in the corrosion resistance of the POS-EP/PDE/CNTs-EP coating can be attributed to the hierarchical structure of the hydrophobic layer and the hydrophilic (underwater oleophobic) layers with the seamless connection.

To better understand the corrosion process of coatings during the immersion test, the equivalent circuits of Fig. S7 were used to fit the EIS data, where R_s represent the solution resistance, Q_c and R_c are the capacitance and resistance of the coating, Q_{dl} and R_{ct} are the double-layer capacitance and charge transfer resistance, respectively. The changes in R_c values can be used to evaluate the barrier ability of the coating against corrosive media [32]. As shown in Fig. 4g, the barrier properties of the coating decreased with immersion time. The R_c value of the EP coating rapidly dropped to 2.52×10^7 Ω cm^2 within 60 days, indicating that the corrosive medium had penetrated the coating. However, throughout the 60-day immersion period, the R_c value of the POS-EP/PDE/CNTs-EP coating remained as high as 5.44×10^9 Ω cm^2 (Fig. 4f), which is significantly higher than FD-POS/EB coating ($R_c = 3.75 \times 10^8$ Ω cm^2) and CNTs-EP coating ($R_c = 2.49 \times 10^8$ Ω cm^2), suggesting the slowest penetration rate of corrosion medium into the coating. To be compared with the functional coatings recently reported, even with the thinner thickness, POS-EP/PDE/CNTs-EP coating still exhibited the advantage in the corrosion resistance reflected by the $|Z|_{0.01Hz}$ value (Fig. 4g) [29,33–36].

The artificial scratches tests were used to examine the protective performance of coatings. As shown in Fig. 5a, after 40 h of immersion, the $|Z|_{0.01Hz}$ value of coatings is 2.13×10^4 Ω cm^2, 1.05×10^6 Ω cm^2, 2.57×10^4 Ω cm$_2$ and 8.05×10^6 Ω cm^2 for EP, POS-EP, CNTs-EP and POS-EP/PDE/CNTs-EP, respectively. The enhancement in the $|Z|_{0.01Hz}$ values of the coatings can be attributed to the presence of a stratified amphiphobic structure. As illustrated in Fig. S8 and Fig. 5b, the Nyquist plot for the POS-EP/PDE/CNTs-EP coating exhibits the largest capacitive arc, indicating that this structure possesses excellent corrosion resistance. Additionally, a new time constant appears at high-frequency in the phase angle plot, suggesting the formation of a novel interface that inhibits the penetration of corrosive media. This can be attributed to the

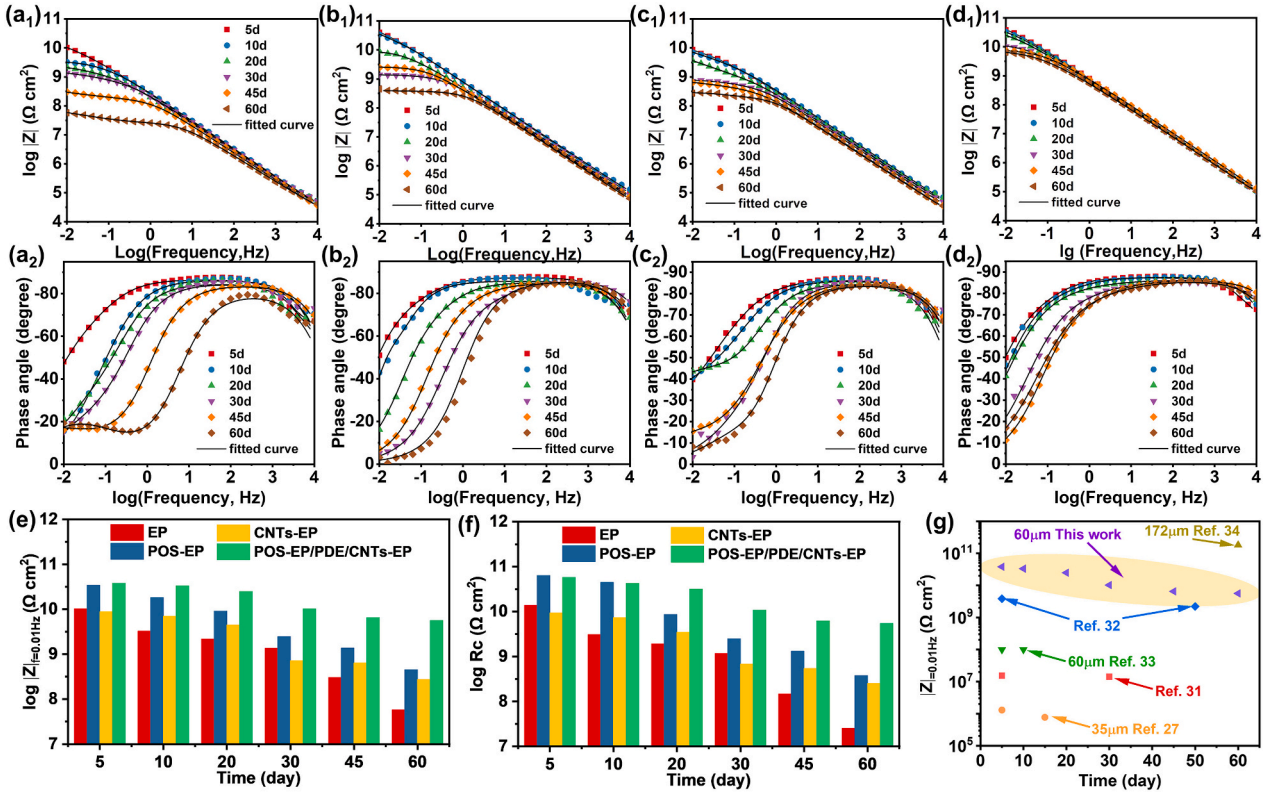

Fig. 4. Bode plots of the coatings immersed in 3.5 wt% NaCl: EP (a1, a2), POS-EP (b1, b2), CNTs-EP (c1, c2) and POS-EP/PDE/CNTs-EP (d1, d2) coatings, Evolution of $|Z|_{0.01Hz}$ (e) and R_c (f) with immersion time, (g) comparison of $|Z|_{0.01Hz}$ value of POS-EP/PDE/CNTs-EP coating with that of previously reported functional coating at different thickness.

"synergistic effect" between the hydrophobic and hydrophilic layers, which creates an additional barrier against the penetration of corrosive media, forming a solid-gas-liquid three-phase interface at the amphoteric boundary. Furthermore, Table S3 presents the fitted impedance data based on the equivalent circuit. The results demonstrate that the R_c value for the POS-EP/PDE/CNTs-EP coating (9.01×10^5 Ω cm^2) is significantly higher than that of POS-EP (3.23×10^5 Ω cm^2), CNTs-EP (1.37×10^4 Ω cm^2), and EP coatings (1.35×10^4 Ω cm^2), confirming the superior corrosion resistance of the amphiphobic coating. The notable increase in the R_c value of the hierarchically amphiphobic coating further underscores the enhancement in barrier performance due to the synergistic effect of the hydrophobic and hydrophilic layers.

Moreover, polarization curve and the fitted results (Fig. 5c and Table S3) showed that POS-EP/PDE/CNTs-EP coating has the most positive corrosion potential of E_{corr} (−0.338 V) and the lowest corrosion current of I_{corr} (1.89×10^{-8} A/cm^{-2}) than the other three coatings of EP (E_{corr} − 0.608 V, I_{corr} 8.67×10^{-7} A·cm^{-2}), CNTs-EP (−0.520 V, 3.49×10^{-7} A·cm^{-2}) and POS-EP (−0.741 V, 1.21×10^{-7} A/cm^2), respectively. The results once again proved that the coating with the hierarchical structure of the hydrophobic POS-EP and the oleophobic CNTs-EP can synergistically block the attacks from the corrosive medium even in the case of the coating being locally broken.

To further ascertain the composition of the corrosion products on the scratched region of Q235 carbon steel after the immersion of 40 h, XPS testing was conducted. As illustrated in Fig. 5d and e. For, the iron elements on the scratched surface can be fitted to five peaks for EP and CNT/EP samples, including Fe (707.9 eV), Fe $2P_{3/2}$ in Fe_2O_3/Fe_3O_4 (709.5 eV), Fe $2P_{3/2}$ in Fe(III) (such as Fe_2O_3/Fe_3O_4), Fe $2P_{1/2}$ (722.3 eV), and Fe $2P_{1/2}$ in Fe(III) (729.7 eV) [34,35]. This is attributed to the poor barrier property of the scratched EP and CNT/EP coatings to corrosive media, which allows the corrosive agents to reach the substrate easily through the scratched areas. Consequently, after 40 h of immersion, the carbon steel surface exhibited a significant amount of corrosion products, primarily composed of $FeCl_2$ and Fe_2O_3/Fe_3O_4.

In contrast, the hydrophobic nature of the POS-EP coating mitigated the penetration of corrosive media. Therefore, the carbon steel surface was predominantly composed of Fe_2O_3/Fe_3O_4 with a minor presence of $FeCl_2$ (Fig. 5f). For the POS-EP/PDE/CNTs-EP coating (Fig. 5g), due to the synergistic effect of the hierarchically amphiphobic structure, the corrosive substances remained isolated away from the substrate, only the Fe_2O_3/Fe_3O_4 peak was detected on the Q235 carbon steel surface. It may be a result of the partial oxidation of Q235 carbon steel during the coating preparation process. Therefore, even with large scratch defects on the coating surface, the penetration of corrosive media was effectively blocked by the synergistic effect of the amphiphobic coating, the Q235 carbon steel was kept in a passive protection state. The result with the electrochemical analyses consistently confirms the excellent corrosion resistance of the POS-EP/PDE/CNTs-EP coating.

To learn the possibility of the synergistic effect, the scratched area of POS-EP-DE/CNTs-EP coating was observed by a photograph. For scratch defects, the Laplace pressure ΔP on the curved liquid interface satisfies follows Eq. (1) [37]

$$\Delta P = -\frac{2\gamma}{r} = \frac{4\gamma \sin(\Psi - \theta)}{R} \quad (1)$$

where r represents the radius of curvature of the bent liquid surface, γ denotes the interfacial tension, θ represents the contact angle, Ψ is the local texture angle (where $\Psi = \theta - \delta\theta$, $\delta\theta$ is the sagging angle of liquid), R is the defect width. As shown in Fig. 5h, when a scratch with a width of 1.0 mm appears on the coating, the aqueous electrolyte first contacts the hydrophilic CNTs-EP coating. At this moment, the local geometric angle (Ψ) of the texture is greater than Young's contact angle (θ) (Fig. 5i). Consequently, the liquid-gas interface exhibits downward additional pressure. This additional pressure can wet the CNTs-EP coating and

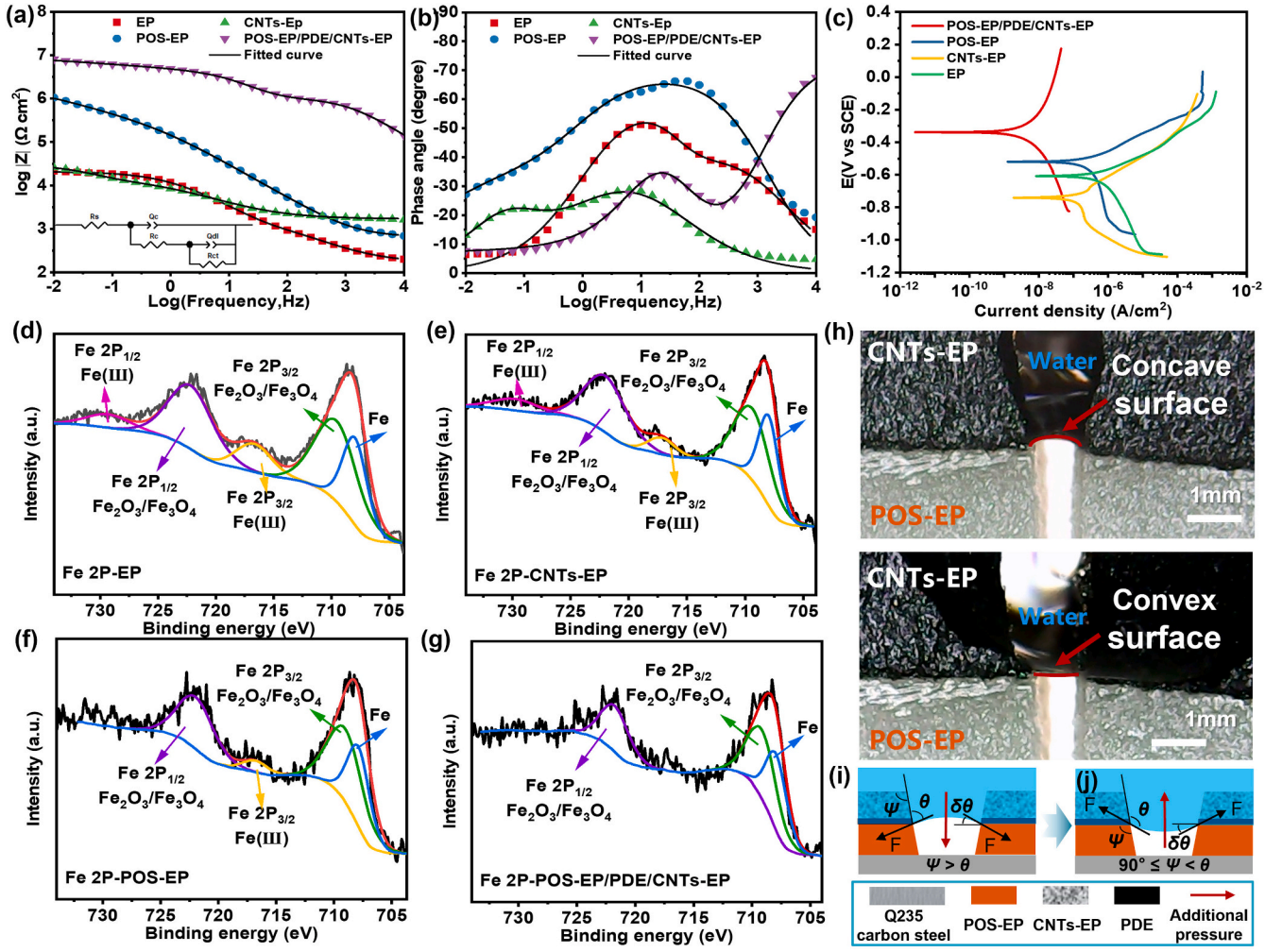

Fig. 5. (a) |Z| vs. frequency of Bode plots, (b) phase angle vs. frequency of Bode plots, (c) polarization curves of scratched EP, POS-EP, CNTs-EP and POS-EP/PDE/CNTs-EP coatings, XPS high-resolution Fe 2p fine spectra of EP (d), POS-EP (e), CNTs-EP (f) and POS-EP/PDE/CNTs-EP (g) coatings, Optical photos (h) and synergistic effect schematic diagram (I, j) of liquid penetration in scratched area of POS-EP/PDE/CNTs-EP coating under macroscopic condition.

drive the liquid to penetrate downward to the interface of the POS-EP coating, thereby forming a concave shape within the gap [6,38].

However, when the electrolyte infiltrates the hydrophobic POS-EP coating interface, the local geometric angle of the texture (Ψ) becomes smaller than the Young's contact angle (θ) (Fig. 5j). The additional pressure is now upward, and this effect is further enhanced by the upward adsorption force from the CNTs-EP coating. The additional pressure tends to drive the liquid-air interface to retreat toward the top edge of the POS-EP coating, forming a convex surface within the gap. This results in a three-phase (solid/air/liquid) interface, creating a Cassie state or transitional state [39,40], which physically blocks the electrolyte's penetration (Fig. 5e). The findings demonstrate that the synergistic effect at the interface of the amphiphobic coating provides an additional pressure for the POS-EP/PDE/CNTs-EP coating, resulting in a notable enhancement of the coating's barrier properties.

Accelerated corrosion tests of neutral salt spray were conducted to evaluate the long-term anti-corrosive performance of coatings. As shown in Fig. 6a, after 10 days test, the EP coating exhibited corrosion spots and wrinkles due to the serious corrosion of the carbon steel. In contrast, the POS-EP and CNTs-EP coatings showed only a few rust spots after 10 days, however, after 18 days, severe corrosion was confined to areas around the rust spots, although modifications with PFDTES and CNTs-COOH on EP significantly enhanced the epoxy resin's resistance to permeation and corrosion. Distinctively, the POS-EP/PDE/CNTs-EP coating remained its anticorrosive property well even after 18 days of salt spray testing, indicating that the effective combination of the POS-EP and CNTs-EP coatings fully utilizes their respective properties to enhance the overall corrosion performance and barrier efficacy of the amphiphobic coating.

To further investigate the penetration process of the corrosive medium within the coatings, EIS tests were conducted on the coatings subjected to the salt spray tests. As illustrated in Fig. 6b, for the EP, POS-EP, and CNTs-EP coatings, the $|Z|_{0.01Hz}$ values exhibit a rapidly decreasing trend over the testing period. After 10 days, the $|Z|_{0.01Hz}$ values decreased to $4.81 \times 10^3\ \Omega\ cm^2$, $7.70 \times 10^4\ \Omega\ cm^2$, and $3.10 \times 10^4\ \Omega\ cm^2$, respectively. This indicates that the corrosive medium has penetrated the carbon steel surface, resulting in corrosion on the coating surface and leading to complete coating failure. Remarkably, the POS-EP/PDE/CNTs-EP coating showcased the exceptional resistance to permeation that maintained a $|Z|_{0.01Hz}$ value of $1.87 \times 10^8\ \Omega cm^2$ even after 18 days of salt spray testing. Notably, a new time constant (0.5 Hz) emerged after 4 days (Fig. 6c), attributing to the corrosive medium reaching the PDE transition layer [31]. Furthermore, the disappearance of the time constant after 8 days of salt spray testing indicated the continued infiltration of the corrosive medium within the coatings. However, the $|Z|_{0.01Hz}$ values remained consistently above $1.0 \times 10^8\ \Omega cm^2$ due to the synergistic effects of the amphiphobic coating, effectively suppressing the penetration of the corrosive medium.

The protective mechanism of the coating was speculated as illustrated in Fig. 6d. For the EP coating, the corrosive medium gradually

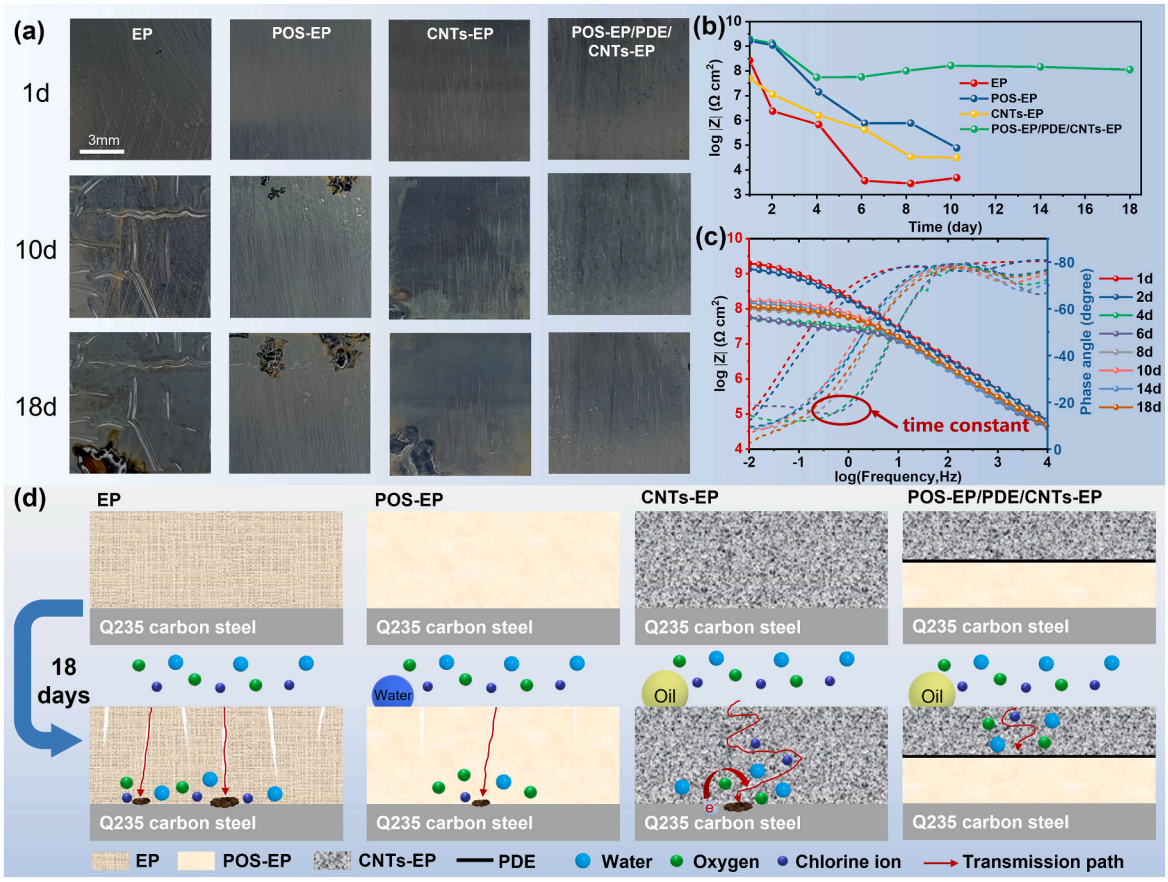

Fig. 6. (a) Optical images of EP, POS-EP, CNTs-EP and FD-POS/EP/PDE/CNTs-EP coatings after 1, 10 and 18 days of salt spray accelerated corrosion testing, (b) Evolution of $|Z|_{0.01Hz}$ with immersion time, (c) Bode plots of POS-EP/PDE/CNTs-EP coating in salt spray accelerated corrosion test, (d) Schematic diagram of anticorrosion mechanism of the coatings.

permeates through the inherent pores and defects formed during the resin curing process over prolonged immersion, leading to metal corrosion. However, PFDTES and CNTs-COOH modifications enhanced the barrier properties of the coating. In the case of the POS-EP coating, the hydrophobicity effectively improves the coating's resistance to hinder the infiltration of corrosive agents and thereby slowing down the corrosion of the coating. Nonetheless, prolonged exposure compromises the hydrophobicity to diminish the coating's permeation resistance. For the CNTs-EP coating, CNTs-COOH can fill the pores and defects within the epoxy resin. Meanwhile, the uniform dispersion of CNTs within the coating extends the diffusion pathway of the corrosive medium, thereby enhancing the coating's barrier effect. Simultaneously, CNTs-COOH increases the hydrophilicity of the coating, resulting in excellent underwater oil-repellent properties, significantly reducing the erosion of the coating by oily pollutants in water. The POS-EP/PDE/CNTs-EP coating, mitigates the adverse effects of hydrophilicity by significantly suppressing the diffusion of corrosive media through the synergistic effect of hydrophilicity and hydrophobicity. Furthermore, the effective protection provided by the CNTs-EP coating prevents the loss of hydrophobicity in the POS-EP coating due to the prolonged exposure. Additionally, the POS-EP coating prevents direct contact between the CNTs and the substrate to shield galvanic corrosion. Therefore, the effective combination of the hydrophobic POS-EP coating and the hydrophilic CNTs-EP coating significantly enhances the barrier properties and corrosion resistance of the coatings.

4. Conclusions

A hierarchically amphiphobic coating constructed by a PFDTES-modified epoxy coating and a CNTs modified epoxy coating which are seamless connected through a PDE transition layer has been successfully explored. The dense CNTs-EP coating with fewer defects can block the corrosive media physically, while its excellent underwater oleophobicity (OCA = 134.6°) significantly reduces the opportunities for various oily pollutants to attack the coating. Furthermore, even the protective property of CNTs-EP coating has locally lost, the underlying POS-EP coating will prevent the attack from the aqueous corrosive ions by the hydrophobic essence. Extremely, once the hierarchically amphiphobic coating was locally broken, the synergistic effect resulted Laplace pressure of ΔP by heterostructure interface between CNT-EP layer and POS-EP layer can hinder the infiltration of electrolyte to protect the metal matrix. Therefore, the hierarchically amphiphobic coating exhibits an extraordinary anticorrosion performance. Electrochemical evaluation and neutral salt spray tests consistently confirmed that the R_c and $|Z|_{0.01Hz}$ of the coating was 2 to 4 orders of magnitude higher than the epoxy resin coatings, the long-term corrosion resistance of the amphiphobic coating outperformed previously reported anti-corrosion coatings and commercial coatings, even with the thinner thickness.

CRediT authorship contribution statement

Zhaowen Tian: Writing – original draft, Software, Methodology, Investigation, Formal analysis, Conceptualization. **Ruiyu Ma:** Software, Methodology, Investigation, Formal analysis, Conceptualization. **Yiqing Chen:** Visualization, Project administration, Investigation. **Suning Li:** Supervision, Investigation, Formal analysis. **Hongwei Zhao:** Validation, Data curation. **Yanqiu Zhang:** Methodology, Investigation, Data curation. **Qingdong Li:** Methodology, Investigation. **Xueyuan Zhang:**

Visualization, Software, Resources. **Baigang An:** Writing – review & editing, Supervision, Resources, Project administration, Funding acquisition, Conceptualization.

Declaration of competing interest

The authors declare that they have no known competing financial interests or personal relationships that could have appeared to influence the work reported in this paper.

Acknowledgments

Financial support by the National Natural Science Foundation of China Nos. 52371224, 51972156 and 51872131 is acknowledged.

Appendix A. Supplementary data

Supplementary data to this article can be found online at https://doi.org/10.1016/j.porgcoat.2025.109186.

Data availability

Data will be made available on request.

References

[1] R. Helbig, J. Nickerl, C. Neinhuis, C. Werner, Smart skin patterns protect springtails, PloS One 6 (9) (2011) e25105.
[2] L. Chen, Z. Guo, W. Liu, Outmatching superhydrophobicity: bio-inspired re-entrant curvature for mighty superamphiphobicity in air, J. Mater. Chem. A 5 (28) (2017) 14480–14507.
[3] Q. Sun, H. He, W.-Y. Gao, B. Aguila, L. Wojtas, Z. Dai, J. Li, Y.-S. Chen, F.-S. Xiao, S. Ma, Imparting amphiphobicity on single-crystalline porous materials, Nat. Commun. 7 (1) (2016) 13300.
[4] P. Zhu, T. Kong, X. Tang, L. Wang, Well-defined porous membranes for robust omniphobic surfaces via microfluidic emulsion templating, Nat. Commun. 8 (1) (2017) 15823.
[5] X. Jiao, M. Li, X. Yu, W.S. Wong, Y. Zhang, Oil-immersion stable superamphiphobic coatings for long-term super liquid-repellency, Chem. Eng. J. 420 (2021) 127606.
[6] Z. Chu, S. Seeger, Superamphiphobic surfaces, Chem. Soc. Rev. 43 (8) (2014) 2784–2798.
[7] Y. Xia, W. Gu, L. Shao, X. Jiao, Y. Ji, W. Deng, X. Yu, Y. Zhang, Y. Zhang, Flexibility and abrasion tolerance of superamphiphobic coatings with rigid core-shell particles, Chem. Eng. J. 476 (2023) 146746.
[8] X. Zhou, J. Liu, W. Liu, W. Steffen, H.J. Butt, Fabrication of stretchable superamphiphobic surfaces with deformation-induced rearrangeable structures, Adv. Mater. 34 (10) (2022) 2107901.
[9] H. Li, Q. Jin, H. Li, H. Tong, K. Wang, S. Chen, G. Ouyang, Z. Wang, Y. Li, Transparent superamphiphobic material formed by hierarchical nano re-entrant structure, Adv. Funct. Mater. 34 (3) (2023) 2309684.
[10] J. Wei, B. Li, N. Tian, J. Zhang, W. Liang, J. Zhang, Scalable robust superamphiphobic coatings enabled by self-similar structure, protective micro-skeleton, and adhesive for practical anti-icing of high-voltage transmission tower, Adv. Funct. Mater. 32 (43) (2022) 2206014.
[11] A. Daneshnia, K. Raeissi, P. Salehikahrizsangi, Corrosion protection of superhydrophobic/amphiphobic cobalt coating with anti-icing and self-cleaning properties fabricated by a one-step electrodeposition method, J. Alloy Compd. 948 (2023) 169767.
[12] W. Li, H. Liu, Novel organic–inorganic hybrid polymer based on fluorinated polyhedral oligomeric silsesquioxanes for stable superamphiphobic fabrics and aluminum corrosion protection, Mater. Today Chem. 29 (2023) 101390.
[13] H. Wang, Z. Zhang, Z. Wang, Y. Liang, Z. Cui, J. Zhao, X. Li, L. Ren, Multistimuli-responsive microstructured superamphiphobic surfaces with large-range, reversible switchable wettability for oil, ACS Appl. Mater. Interfaces 11 (31) (2019) 28478–28486.
[14] X. Ou, J. Cai, J. Tian, B. Luo, M. Liu, Superamphiphobic surfaces with self-cleaning and antifouling properties by functionalized chitin nanocrystals, ACS Sustain. Chem. Eng. 8 (17) (2020) 6690–6699.
[15] N. Abu Jarad, H. Imran, S.M. Imani, T.F. Didar, L. Soleymani, Fabrication of superamphiphobic surfaces via spray coating; a review, Adv. Mater. Techno. 7 (10) (2022) 2101702.
[16] Z. Zhao, S. Liu, C. Sun, Y. Wu, D. Zhang, A novel epoxy-based self-healing robust superhydrophobic coatings for oil/water separation, Prog. in Org. Coat. 194 (2024) 108574.
[17] J. Wei, B. Li, L. Jing, N. Tian, X. Zhao, J. Zhang, Efficient protection of Mg alloy enabled by combination of a conventional anti-corrosion coating and a superamphiphobic coating, Chem. Eng. J. 390 (2020) 124562.
[18] X. Zhao, D.S. Park, J. Choi, S. Park, S.A. Soper, M.C. Murphy, Flexible-templated imprinting for fluorine-free, omniphobic plastics with re-entrant structures, J. Colloid. Interf. Sci. 585 (2021) 668–675.
[19] H. Zhao, K.-Y. Law, V. Sambhy, Fabrication, surface properties, and origin of superoleophobicity for a model textured surface, Langmuir 27 (10) (2011) 5927–5935.
[20] M. Im, H. Im, J.-H. Lee, J.-B. Yoon, Y.-K. Choi, A robust superhydrophobic and superoleophobic surface with inverse-trapezoidal microstructures on a large transparent flexible substrate, Soft Matter 6 (7) (2010) 1401–1404.
[21] H. Kim, K. Noh, C. Choi, J. Khamwannah, D. Villwock, S. Jin, Extreme superomniphobicity of multiwalled 8 nm TiO_2 nanotubes, Langmuir 27 (16) (2011) 10191–10196.
[22] G. Liu, H. Xia, W. Zhang, L. Lang, H. Geng, L. Song, Y. Niu, Photocatalytic superamphiphobic coatings and the effect of surface microstructures on superamphiphobicity, ACS Appl. Mater. Interfaces 13 (10) (2021) 12509–12520.
[23] H. Du, F. Liu, H. Wang, Bio-inspired robust superhydrophilic/underwater superoleophobic coating with lubrication, anti-crude oil fouling and anti-corrosion performances, J. Colloid. Interf. Sci. 616 (2022).
[24] Y. Li, W. Ma, Y.S. Kwon, W. Li, S. Yao, B. Huang, Solar deicing nanocoatings adaptive to overhead power lines, Adv. Funct. Mater. 32 (25) (2022) 2113297.
[25] S. Wang, K. Liu, X. Yao, L. Jiang, Bioinspired surfaces with superwettability: new insight on theory, design, and applications, Chem. reviews 115 (16) (2015) 8230–8293.
[26] X. Luo, J. Zhong, Q. Zhou, S. Du, S. Yuan, Y. Liu, Cationic reduced graphene oxide as self-aligned nanofiller in the epoxy nanocomposite coating with excellent anticorrosive performance and its high antibacterial activity, ACS Appl. Mater. Interfaces 10 (21) (2018) 18400–18415.
[27] X. Zhu, H. Zhao, L. Wang, Q. Xue, Bioinspired ultrathin graphene nanosheets sandwiched between epoxy layers for high performance of anticorrosion coatings, Chem. Eng. J. 410 (2021) 128301.
[28] X. Yang, X. Zhong, J. Zhang, J. Gu, Intrinsic high thermal conductive liquid crystal epoxy film simultaneously combining with excellent intrinsic self-healing performance, J. Mater. Sci. Technol. 68 (2021) 209–215.
[29] Y. Ma, H. Huang, H. Zhou, M. Graham, J. Smith, X. Sheng, Y. Chen, L. Zhang, X. Zhang, E. Shchukina, Superior anti-corrosion and self-healing bi-functional polymer composite coatings with polydopamine modified mesoporous silica/graphene oxide, J. Mater. Sci. Technol. 95 (2021) 95–104.
[30] S. Dong, Y. Li, N. Tian, B. Li, Y. Yang, L. Li, J. Zhang, Scalable preparation of superamphiphobic coatings with ultralow sliding angles and high liquid impact resistance, ACS Appl. Mater. Interfaces 10 (49) (2018) 41878–41882.
[31] X. Zhu, H. Zhao, L. Wang, Q. Xue, Bioinspired ultrathin graphene nanosheets sandwiched between epoxy layers for high performance of anticorrosion coatings, Chem. Eng. J. 410 (2021) 128301.
[32] X. Zhu, Q. Yan, L. Cheng, H. Wu, H. Zhao, L. Wang, Self-alignment of cationic graphene oxide nanosheets for anticorrosive reinforcement of epoxy coatings, Chem. Eng. J. 389 (2020) 124435.
[33] X. Liu, P. Hou, X. Zhao, X. Ma, B. Hou, The polyaniline-modified TiO_2 composites in water-based epoxy coating for corrosion protection of Q235 steel, J. Coat. Technol. Res. 16 (2019) 71–80.
[34] L. Cheng, H. Wu, J. Li, H. Zhao, L. Wang, Polydopamine modified ultrathin hydroxyapatite nanosheets for anti-corrosion reinforcement in polymeric coatings, Corros. Sci. 178 (2021) 109064.
[35] D. Xue, Q.B. Meng, Y.X. Lu, L. Liang, Y.H. Wei, X.B. Liu, Achieving high performance anticorrosive coating via in situ polymerization of polyurethane and poly (propylene oxide) grafted graphene oxide composites, Corros. Sci. 176 (2020) 109055.
[36] X. Wang, Y. Li, C. Li, X. Zhang, D. Lin, F. Xu, Y. Zhu, H. Wang, J. Gong, T. Wang, Highly orientated graphene/epoxy coating with exceptional anti-corrosion performance for harsh oxygen environments, Corros. Sci. 176 (2020) 109049.
[37] Z. Zhao, Y. Ning, S. Ben, X. Zhang, Q. Li, C. Yu, X. Jin, K. Liu, L. Jiang, Liquid-assisted single-layer janus membrane for efficient unidirectional liquid penetration, Adv. Sci. 9 (2) (2022) 2103765.
[38] A. Tuteja, W. Choi, M. Ma, J.M. Mabry, S.A. Mazzella, G.C. Rutledge, G. H. McKinley, R.E. Cohen, Designing superoleophobic surfaces, Science 318 (5856) (2007) 1618–1622.
[39] Y. Sun, Z. Guo, Recent advances of bioinspired functional materials with specific wettability: from nature and beyond nature, Nanoscale Horiz. 4 (1) (2019) 52–76.
[40] A. Tuteja, W. Choi, J.M. Mabry, G.H. McKinley, R.E. Cohen, Robust omniphobic surfaces, Proc. Natl. Acad. Sci. 105 (47) (2008) 18200–18205.